Chemical termination of the CsCl-structure FeSi/Si(111) film surface and its multilayer relaxation

S. Walter, R. Bandorf, W. Weiss, and K. Heinz
Lehrstuhl für Festkörperphysik, Universität Erlangen-Nürnberg, Staudtstrasse 7, D-91058 Erlangen, Germany

U. Starke
Max-Planck-Institut für Festkörperforschung, Heisenbergstrasse 1, D-70569 Stuttgart, Germany
and Lehrstuhl für Festkörperphysik, Universität Erlangen-Nürnberg, Staudtstrasse 7, D-91058 Erlangen, Germany

M. Strass, M. Bockstedte, and O. Pankratov
Lehrstuhl für Theoretische Festkörperphysik, Universität Erlangen-Nürnberg, Staudtstrasse 7, D-91058 Erlangen, Germany
(Received 30 July 2002; published 21 February 2003)

Metallic FeSi films, epitaxially stabilized on Si(111) in CsCl structure, are investigated experimentally by quantitative low-energy electron diffraction (LEED) and theoretically by total energy calculations using density functional theory (DFT). Both methods show clearly that the surface is Si terminated. Additionally, LEED and DFT agree in retrieving an unusual multilayer relaxation of $+6\%$, -16%, and $+14\%$ from the top layer into the bulk for the first three layer spacings. This relaxation pattern is explained by an enhanced covalent bonding between the subsurface iron and silicon layers.

DOI: 10.1103/PhysRevB.67.085413 PACS number(s): 68.35.Bs

I. INTRODUCTION

For more than a decade metal silicides grown epitaxially on silicon have been attracting intensive attention owing to their potential importance for silicon-based device technology.[1] This applies in particular to iron silicide grown on Si(111) which shows, dependent on the stoichiometry, a considerable variety of structures[2] with different properties. Especially in the regime of ultrathin films, phases that are unstable as bulk structures can be synthesized exhibiting new and unexpected properties such as, e.g., supersoftness.[3] A bulk-unstable CsCl-type phase of FeSi was first reported by von Känel *et al.*[4] and confirmed in later investigations.[5,6] It can be related to the bulk-stable B20 structure (ε-FeSi) via a trigonal distortion and relaxation of internal coordinates.[7] In thin films the CsCl phase becomes more stable than ε-FeSi due to the smaller lattice mismatch with the substrate (2% compared to -6.4% for ε-FeSi) and consequently the smaller elastic energy of the strained film.[3,8] This so-called *c*-FeSi (Ref. 9) structure shows metallic character and as such may be used for manufacturing electric contacts on silicon. *c*-FeSi films of up to 10^3 Å thickness can be prepared by stoichiometric codeposition of Fe and Si.[4]

For applications in microelectronics, the properties of the material with respect to environmental influences are especially important. These properties certainly depend on the films surface structure, in particular the chemical termination which, in (111) film orientation, can be either by Fe or Si layers. Yet investigations of the atomic surface structure are scarce. By comparison of measured and semiempirically calculated electronic band structures, Hinarejos *et al.* indirectly concluded that the topmost *c*-FeSi layer was Fe, a result which seemed to be supported by ion scattering spectroscopy (ISS) as published in the same paper.[6] On the other hand, Junquera *et al.* recently reevaluated the very same experimental band structure data by comparison to *ab initio* calculations and concluded that the surface should be Si terminated.[10] This makes the whole issue of the chemical termination rather contradictory.

In the present paper we resolve the problem by the joint application of experimental and theoretical structure determination techniques. On the experimental side, we use quantitative low-energy electron diffraction (LEED) which, in addition to the crystal structure and surface termination, resolves the multilayer relaxation beneath the surface. Theoretically, total energy calculations by means of density functional theory (DFT) are producing the same structural parameters. With the chemical potential being adjusted to the experimental situation, theory and experiment impressively agree: The surface is undoubtedly terminated by Si. It shows a multilayer relaxation, which is unusual with respect to the sign and relative size of relaxations of the top few layer spacings. We offer a physical explanation of our results based on the analysis of the surface bonding by calculating the local electronic density of states.

The experimental approach, including sample preparation, LEED data acquisition, and intensity analysis, is described in Sec. II. In Sec. III, the theory is outlined and the resulting electronic structure and energetic properties of the surface are presented. In Sec. IV a comparison and discussion of the results achieved experimentally and theoretically are given. Finally, Sec. V concludes the paper.

II. LEED STRUCTURE ANALYSIS

A. Sample preparation and measurements

The preparation of the films and the measurements were carried out in an ultrahigh-vacuum (UHV) chamber equipped with a reverse-view LEED optics and a 150° hemispherical analyzer for Auger electron spectroscopy (AES). As substrate, silicon pieces of 6×12 mm^2 size were cut from a (111)-oriented wafer of 0.5 mm thickness. They were prepared *in situ* by resistive heating, resulting in a clean, well-ordered (7×7)-Si(111) surface as verified by LEED and AES. The sample temperature was measured by means of a W/Re thermocouple which was attached to the sample's back and calibrated through an infrared pyrometer. Iron and sili-

 ©2003 The American Physical Society

con were coevaporated using electron-heated solid-source evaporators with a quartz balance to control the evaporation rate. Compared to evaporation of iron alone and subsequent silicidation by annealing, this coevaporation leads to films of higher quality as evidenced by sharper diffraction spots and lower background in the LEED pattern.[11] Deposition of Fe and Si in the stoichiometric 1:1 ratio followed by thermal annealing at 300 °C (approximately 10 min) makes the initially (7×7) superstructure of clean Si(111) disappear. Instead, a (1×1) pattern develops whose quality was optimized by adjusting the annealing time. The 1:1 stoichiometry of the film formed was confirmed by AES. The deposition of eight monolayers (ML) of Fe and the equivalent of Si resulted in a silicide film of an approximate thickness of 13 Å (layer spacing approximately 0.8 Å).

Intensity versus energy spectra $I(E)$ of LEED spots were recorded in UHV with a fast, video-based data acquisition system.[12] During the measurement, the sample was cooled to liquid nitrogen temperature in order to reduce thermal diffuse scattering. Normal incidence of the primary electron beam was adjusted by comparing the spectra of beams which are symmetry equivalent at this incidence such as, e.g., beams $(0,1)$, $(1,\bar{1})$, and $(\bar{1},0)$. For the final data set, the influence of residual misalignment and inhomogeneities of the luminescent screen was further reduced by averaging of equivalent spectra. The resulting database included seven symmetrically inequivalent beams whose spectra cover a total energy width of $\Delta E = 1900$ eV.

B. Intensity calculations and structural search

The computation of LEED $I(E)$ spectra was performed using the TensErLEED program package.[13] This is based on the tensor LEED perturbation method[14–16] allowing for the fast variation of structural and nonstructural parameters. The best fit structure, i.e., the configuration in parameter space whose spectra fit best to the measured data, was found by an automated structural search procedure[17] guided by the Pendry R factor R_P.[18] Error limits were estimated by the variance of the R factor, $\mathrm{var}(R_P) = R_P^{min}\sqrt{8V_{0i}/\Delta E}$, with $V_{0i} = 6$ eV the imaginary part of the inner potential describing electron attenuation. Possible correlations between parameters were neglected within the error estimation. The atomic scattering for energies up to 450 eV was described by up to nine fully relativistic and spin-averaged phase shifts. They were corrected for thermal vibrations and possible static positional disorder described by mean-square displacements (MSD's) off the lattice sites. Different MSD's were allowed for atoms in the topmost layer, second layer, and for atoms below. For the real part of the inner potential, V_{0r}, it was shown earlier that neglect of its energy dependence—which is due to the variation of the exchange-correlation potential—may lead to systematic errors in the resulting structural parameters.[19] Thus, its energy dependence was taken into account which, following Ref. 20, can be approximated by[21] $V_{0r}(E) = V_{00} + \max(0.49 - 92.55/\sqrt{(E/\mathrm{eV}) + 18.51}, -11.33)\mathrm{eV}$. This energy dependence was considered both for the calculation of phase shifts[21] and the fit between experimental and calculated data, whereby V_{00} was allowed to vary.

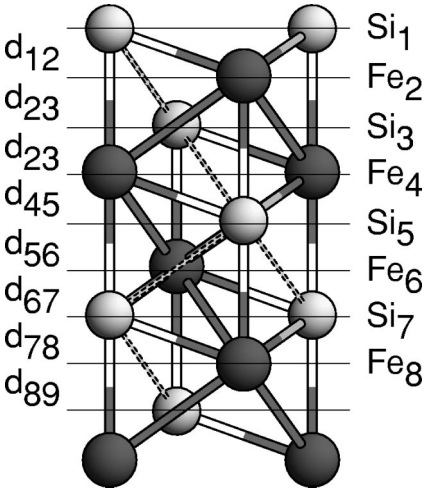

FIG. 1. Side view of a (111)-oriented film of Si-terminated c-FeSi projected perpendicular to the $\{\bar{1}10\}$ plane. Dark spheres represent Fe atoms, light spheres Si atoms. Fe-Fe and Fe-Si bonds are shaded according to the connected elements. Si-Si connections are drawn as thin dashed lines for a clear three-dimensional (3D) view. Element subscripts correspond to their subsurface depth on the right; interlayer spacings are indicated on the left.

The usual procedure to stack layers in the plane-wave representation of the wave field fails for the present case, since the interlayer spacing in the [111] direction is smaller than 1 Å, which causes numerical instabilities.[22] These are avoided when scattering in the full surface probed by the electrons is described by spherical waves, i.e., by treating the full surface as a single composite layer with the number of atomic planes determined by electron attenuation. Of course, the price to pay for this improved accuracy is a substantially increased computing time, since a large matrix has to be inverted. The thickness of the surface slab used was carefully checked for convergence. A total of 14 atomic planes equivalent to a thickness of about 11 Å proved to be sufficient; i.e., for thicker slabs the spectra remained practically unchanged as checked by the R factor.

The models tested where all of CsCl-type structure since this crystal structure had been determined independently by a variety of methods.[4–6,9] The silicon substrate needed not to be included in the calculations since it is approximately 13 Å below the film surface. From this depth—consistent with the above-mentioned convergence of the slab calculation as a function of the slab thickness—virtually no LEED electrons reach the surface by backscattering due to electron attenuation. In the [111] direction, CsCl-type FeSi can be considered as stacked from layers alternatingly composed of Fe and Si, as indicated in Fig. 1. Hence, the surface is terminated either by a Si or Fe layer. A mixture of Si- *and* Fe-terminated domains can be excluded as the surface has been shown to exhibit steps of only double atomic height.[4,8] Accordingly, Fe- and Si-terminated surfaces could be tested independently in the calculations. Additionally, the vertical spacings $d_{i,i+1}$ between adjacent layers ($i = 1$ denotes the top layer; cf. Fig.

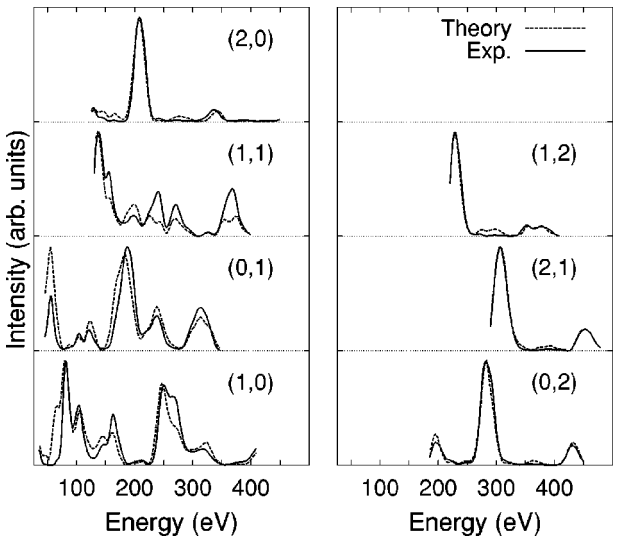

FIG. 2. Comparison of experimental (solid lines) and best-fit calculated (dotted lines) $I(E)$ spectra.

1) were varied down to $i=8$. For layers below, a common spacing $d_0=0.805$ Å was used as resulting from x-ray diffraction of very thick films[23] and from *ab initio* total energy calculations.[3] All atoms were allowed to vibrate isotropically whereby MSD's for atoms in the first and second layers as well as for Fe and Si atoms below were varied independently.

C. Structural results

For the search within the parameter space of an Fe-terminated surface, always $R_P \geqslant 0.33$ resulted. In contrast, the fit of spectra of a Si-terminated *c*-FeSi crystal to the experimental data is of much higher quality as reflected by an *R* factor $R_P^{\min}=0.17$ and a favorable visual comparison of spectra as displayed in Fig. 2. Thus, an unambiguous decision can be made in favor of the Si-terminated *c*-FeSi phase, since structures leading to R_P values higher than $[R_P^{\min} + \mathrm{var}(R_P)]=0.20$ can be ruled out by statistical arguments.[18]

Before addressing the best-fit structure displayed in Table I, we address the issue of error limits which are also given in the table. They are rather large for the top-layer spacing due to the increased vibrational amplitude determined for top Si atoms (0.14 Å) and their weak scattering compared to Fe.

TABLE I. Best-fit values for the interlayer spacings d_{ij} (left) and their relaxations relative to the bulk value d_0 (right). See Fig. 1 for the labeling.

d_{12} (Å)	0.85 ± 0.04	$\Delta d_{12}/d_0$ (%)	$+6\pm5$
d_{23} (Å)	0.68 ± 0.02	$\Delta d_{23}/d_0$ (%)	-16 ± 2
d_{34} (Å)	0.92 ± 0.02	$\Delta d_{34}/d_0$ (%)	$+14\pm2$
d_{45} (Å)	0.78 ± 0.02	$\Delta d_{45}/d_0$ (%)	-3 ± 2
d_{56} (Å)	0.82		
d_{67} (Å)	0.81		
d_{78} (Å)	0.79		
d_{89} (Å)	0.82		

Second-layer Fe atoms still vibrate considerably (0.12 Å), but due to their higher scattering strength and the reduced vibrational amplitudes in the next layers (Si:0.09 Å; Fe:0.08 Å), the next few spacings can be determined with higher accuracy in spite of the electron attenuation. Of course the latter causes increasing error limits for even deeper layers. It should be noted that the vibrational amplitudes of surface atoms being by a factor of about 1.5 larger than bulk amplitudes is consistent with common experience.

The best-fit structure shows a pronounced multilayer relaxation down to the fourth spacing as displayed in Table I (see the right column for relative deviations from the bulk value). Deeper spacings agree with the bulk value d_0 within the statistical limits of errors. Compared to bcc-type elemental metal or alloy surfaces of (111) orientation, which due to the openness of the surface exhibit a $(--+)$ sequence of layer relaxations,[24–27] the $(+-+)$ sequence observed for *c*-FeSi is rather unusual, in particular the expansion of the top spacing. While the large contraction of the second spacing fits to the general pattern, this does not hold for the strong expansion of the third spacing. Obviously, the response of the surface to the breaking of bonds suffered by surface atoms is not controlled by delocalized electrons, even though *c*-FeSi is metallic. To gain a deeper understanding of these observations, *ab initio* calculations were conducted as presented in the next section.

III. THEORETICAL ANALYSIS

A. *Ab initio* method

For the theoretical analysis of the FeSi surface, the *ab initio* pseudopotential plane-wave method FHI96SPIN (Ref. 28) based on density functional theory is employed. The generalized gradient approximation (GGA) of Perdew and Wang[29] is used for the description of the exchange-correlation functional. To account for possible magnetic effects, a spin polarization is allowed in all calculations.

Due to the relatively large thickness of FeSi films in the experiment, the effect of the interface can be neglected. In other words, a perfect strain-free interface without any electronic coupling to the substrate is assumed. The film is thus modeled as a free-standing FeSi (111) slab. This FeSi slab consists of 15 atomic layers, and a vacuum region corresponding to the thickness of 16 atomic layers is used. Soft norm-conserving pseudopotentials of the Troullier-Martin type have been constructed with the help of the FHIPP package[30] including a pseudocore for the description of the nonlinear core-valence exchange and correlation interaction,[31] which is especially important for iron.[32]

A standard silicon pseudopotential[33] and a softened iron potential[34,35] (ps1) were employed, which allowed an energy cutoff of 70 Ry for the plane-wave basis set. The performance of this potential was carefully compared to a harder version[36] (ps2) using bulk and surface properties. For the lattice constant ($a_0=2.80$ Å) and the bulk modulus ($B_0=2.16$ Mbar) virtually the same results are obtained with the two potentials. The lattice constant is in good agreement with the experimental value[23] ($a_{expt}=2.77$ Å). Also, a comparison with other calculations underlines the eligibility of our

pseudopotentials. Applying an ultrasoft pseudopotential method within the GGA, the recent work of Moroni *et al.*[7] provides the values $a_0^{GGA}=2.77$ Å and $B_0^{GGA}=2.21$ Mbar. Their local density approximation (LDA) result ($a_0^{LDA}=2.72$ Å, $B_0^{LDA}=2.63$ Mbar) is consistent with the general trend of overbinding in LDA calculations. As pointed out by Moroni *et al.* the ground-state energy within the GGA fits in comparison with the LDA results substantially better with experiment.

A satisfactory energetic description using the softened potential ps1 is also verified. For the heat of formation of *c*-FeSi, we obtain a value of $H_{FeSi}=-0.28$ eV per atom using this potential compared to -0.31 eV for the potential ps2. This result is in agreement with the value of -0.38 eV obtained by Moroni *et al.*[7] within the GGA. Since *c*-FeSi is not a bulk-stable phase, no experimental values exist for H_{FeSi}. Therefore, we use ferromagnetic Fe_3Si as a reference. A similar performance of the two potentials is found for Fe_3Si (ps1: -0.21 eV; ps2: -0.20 eV) in comparison to the value of Ref. 7 (-0.28 eV). An excellent agreement with the experimental value[37] of -0.21 eV is obtained.

Concerning the surface properties, explicit tests for the (111) surface were not feasible. Nevertheless, a comparison of the relaxation of a Si-terminated (100) surface shows good agreement between the results obtained with the two pseudopotentials ps1 and ps2, except for the relaxation of the first two layers, which is slightly larger for the softer potential ps1 ($d_{12}=1.55$ Å and $d_{23}=1.33$ Å compared to $d_{12}=1.47$ Å and $d_{23}=1.37$ Å).

All calculations have been performed using a **k**-point sampling within the Monkhorst-Pack scheme[38] including 12 **k**-points in the irreducible wedge of the Brillouin zone and an energy cutoff of 70 Ry. The film has been described using either the intrinsic lattice constant of *c*-FeSi or that of silicon for the lateral lattice constant. In both cases, the same layer relaxation was found despite the lattice mismatch of 2% of the unstrained FeSi(CsCl) with the Si substrate. This is a consequence of the epitaxial softness of the CsCl phase.[3]

B. Energetically preferred surface termination

The stabilization of the FeSi surface is controlled by the energetics of the different terminations, but may be influenced by kinetic processes during the preparation of the film. A partial equilibrium between the substrate and film can be obtained, provided the mass transport is not suppressed and the desorption from the film surface is not relevant. The surface termination is then determined by the energetic criterion; i.e., the termination with the lowest surface tension dominates. The surface tension γ of the alloy *c*-FeSi is given by the Gibbs free energy *G* of the film and depends on the chemical potentials μ_{Fe} and μ_{Si} of iron and silicon. It reads

$$\gamma=\frac{1}{A}[G(T,n_{Fe},n_{Si})-n_{Fe}\mu_{Fe}-n_{Si}\mu_{Si}], \qquad (1)$$

where *A* is the area of the surface unit cell and n_{Fe} and n_{Si} are the number of Fe and Si atoms. In equilibrium, μ_{Fe} and μ_{Si} are related to the chemical potential of *c*-FeSi by $\mu_{Fe}+\mu_{Si}=\mu_{FeSi}$. For our symmetric (111) slabs with two equivalent surfaces a direct evaluation of γ using Eq. (1) is possible. Approximating the Gibbs free energy by the total energy of the slab and expressing μ_{Si} by its deviation from the bulk value, $\Delta\mu_{Si}=\mu_{Si}-\mu_{Si}^0$, the surface tension is calculated as

$$\gamma(\Delta\mu_{Si})=\frac{1}{2A}[E_0^{slab}-(n_{Si}-n_{Fe})\Delta\mu_{Si}], \qquad (2)$$

where $E_0^{slab}=E_{tot}^{slab}-n_{Fe}\mu_{FeSi}-(n_{Si}-n_{Fe})\mu_{Si}^0$ is obtained from the total energy of the slab, E_{tot}^{slab}, and the total energy per chemical unit of *c*-FeSi, μ_{FeSi}, and silicon, μ_{Si}^0; the factor of 2 accounts for the presence of two surfaces.

The variation of $\Delta\mu_{Si}$ is limited by the existence of other stable phases. The upper boundary is given by the formation of the elemental silicon phase ($\Delta\mu_{Si}=0$). The lower boundary is imposed by the formation of other Fe-rich silicide phases or the segregation of elemental Fe, which implies that $\Delta\mu_{Si}$ cannot have values below the heat of formation, H_{FeSi}, of *c*-FeSi. Our results for the surface tension of the Si- and Fe-terminated surface are shown in Fig. 3.

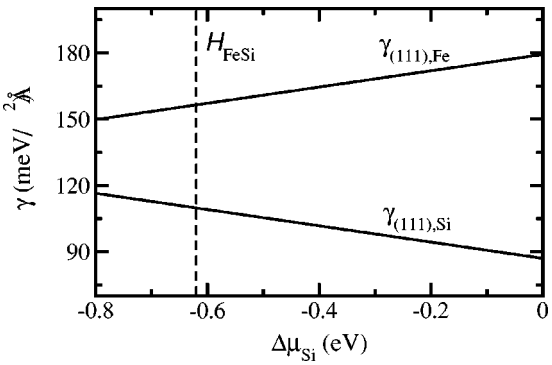

FIG. 3. Surface tension $\gamma_{(111),Si}$ and $\gamma_{(111),Fe}$ vs chemical potential $\Delta\mu_{Si}$ for the Si- and Fe-terminated surfaces. The lower boundary for $\Delta\mu_{Si}$ as approximated by H_{FeSi} per formula unit (obtained with the potential ps2; see text) is indicated by the dashed line.

For the FeSi film and the Si substrate being in equilibrium ($\Delta\mu_{Si}\lesssim 0$), the surface tension $\gamma_{(111),Si}$ of the Si-terminated surface is smaller than $\gamma_{(111),Fe}$ of the Fe termination. The Si-terminated surface is energetically preferred. The difference between $\gamma_{(111),Fe}$ and $\gamma_{(111),Si}$ for this special case amounts to 93 meV/Å^2 or 1.25 eV per surface unit cell. Even under a pronounced Fe excess ($\Delta\mu_{Si}=H_{FeSi}$) the Si termination remains more favorable by 45 meV/Å^2 or 0.61 eV per surface unit cell compared to the Fe termination.

C. Bonding of *c*-FeSi and the local density of states

For the Si- and Fe-terminated surfaces our calculations reveal different types of relaxations. The layer spacings are listed in Table II. While the Si-terminated surface exhibits a $(+-+-)$ relaxation sequence, the Fe-terminated surface shows a $(-++-)$ sequence. The driving force behind these relaxation patterns is the surface electronic structure. Before entering a detailed discussion in the following sections, we briefly outline the general aspects of bonding in FeSi and the

TABLE II. Theoretical results for the interlayer spacings d_{ij} of Si- and Fe-terminated (111) surfaces and their relaxation relative to the bulk value $d_0 = 0.81$ Å. The index at the element refers to the layer number (surface layer: $i = 1$). Our results are compared with those of Ref. 10.

Si termination				Fe termination			
	d_{ij} (Å)	$\Delta d/d_0$ (%)			d_{ij} (Å)	$\Delta d/d_0$ (%)	
Si_1-Fe_2	0.85	+5	+9[a]	Fe_1-Si_2	0.47	−42	−13[a]
Fe_2-Si_3	0.58	−28	−16[a]	Si_2-Fe_3	0.91	+14	+5[a]
Si_3-Fe_4	1.01	+25	+10[a]	Fe_3-Si_4	0.88	+8	−1[a]
Fe_4-Si_5	0.76	−6	−1[a]	Si_4-Fe_5	0.75	−7	+5[a]
Si_5-Fe_6	0.83	+3	–	Si_5-Fe_6	0.76	−1	–

[a]Reference 10, DFT-LDA slab calculations.

interpretation of the surface electronic structure via the local electronic density of states (LDOS).

For the relatively open (111) surface the atomic coordination at the surface differs drastically from the eightfold coordination in the bulk as indicated in Fig. 4. While atoms in the surface layer miss four nearest neighbors and three second-nearest neighbors [panel (a)], one nearest neighbor and three second-nearest neighbors are missed by second-layer atoms [panel (b)]. In the third layer the coordination is still reduced by one nearest neighbor [panel (c)]. This implies a considerable rearrangement of the electronic structure at the surface, in particular for the overcoordinated silicon.

Mäder *et al.*[39] have described the bonding of *c*-FeSi in terms of Fe-Fe bonds and Fe-Si bonds. Each Fe atom forms strong bonds with its six Fe neighbors via σ bonds (d_{z^2} and $d_{x^2-y^2}$ orbitals) and π bonds (d_{xy}, d_{xz}, and d_{yz} orbitals). Weaker Fe-Si bonds are formed between *p* orbitals of the eightfold-coordinated Si and the Fe d_{xy}, d_{xz}, and d_{yz} orbitals. In contrast to γ-$FeSi_2$ which has a CaF_2 structure with dominating Fe-Si bonds, the *p*-*d* bonding in *c*-FeSi is less

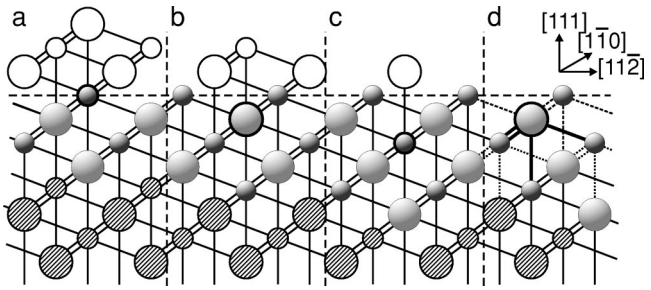

FIG. 4. Projected geometry and bonding of surface and subsurface atoms at the *c*-FeSi(111) surface. (a)–(c) Reduced coordination of the atoms indicated by the thick outlined spheres; white spheres represent neighbors removed due to the truncation of the bulk crystal. (d) Bond enhancement (thick lines) and weakening (dashed and dotted lines). Bonds within the $\{1\bar{1}0\}$ projection plane are drawn as single lines; double lines indicate two bonds directed by 60° into and out of the plane. Large spheres represent Fe atoms and small spheres Si atoms. Hatched spheres are not included in the discussion. The surface is indicated by the horizontal dashed line; panels are separated by vertical dashed lines.

pronounced as the quantitative analysis of Mäder *et al.* shows. The weak *p*-*d* mixing can be qualitatively related to the specific crystal symmetry. In the Brillouin zone center it is strictly forbidden, so that only the states with finite quasimomentum can contribute to the *p*-*d* bonding. However, the *p*-*d* interaction is important to explain the ordering of the band structure[39] and the existence of the surface band gaps in the projected band structure of the (111) film surface.[10] The Fermi level falls into the region of a low density of states below a *d*-band peak originating from antibonding Fe-Fe-bonds consistent with the crystal-field splitting. As a consequence, the low density of states at the Fermi level is hindering a magnetic ordering in FeSi. In the bulk-stable ε-FeSi-phase, which is by 0.07 eV per formula unit more stable, this pseudogap results in a real gap in the LDOS as discussed in Ref. 7. The CsCl phases and ε-FeSi are connected via a trigonal distortion of the CsCl lattice along the [111] axis towards the rocksalt structure (which is unstable) and an additional relaxation of internal coordinates.

The role of covalent binding in the surface relaxation is revealed by the LDOS. The latter is given by

$$D_{ilm}(E) = \sum_{\nu} \int_{\mathrm{BZ}} d^2k |\langle \Psi_{\nu\mathbf{k}} | \Phi_{i\mathbf{k}lm} \rangle|^2 \delta(E - E_{\nu\mathbf{k}}), \quad (3)$$

where the sum and integration over the surface Brillouin zone run over all Kohn-Sham orbitals $\Psi_{\nu\mathbf{k}}$ with Kohn-Sham eigenvalues $E_{\nu\mathbf{k}}$. The functions $\Phi_{i\mathbf{k}lm}(\mathbf{r})$ are the Bloch sums $\Sigma_{\mathrm{R}} \exp[\imath\mathbf{k}\cdot(\mathbf{R}+\mathbf{R}_i)]\phi_{ilm}(\mathbf{r}-\mathbf{R}-\mathbf{R}_i)$ of the contracted atomic pseudowave function[40] ϕ_{ilm} with quantum numbers *l* and *m* that is located in the *i*th layer at $\mathbf{R}_i$. Note that the LDOS includes a sum over the two spin states. Equation (3) is numerically evaluated by replacing the δ function with a Gaussian (full width at half maximum of 0.13 eV). The Brillouin zone integration is performed as a summation over a **k**-point mesh with a total of 113 **k** points.

By the symmetry of the (111) surface, the Fe *d* orbitals are grouped in the pairs $d_{xy}/d_{x^2-y^2}$ and d_{xz}/d_{yz} with the d_{z^2} orbital remaining unpaired. The d_{z^2} orbital promotes a σ bonding with its two Si neighbors along the [111] axis. Combinations of d_{z^2} with the other two groups of *d* orbitals form the bulklike Fe-Fe σ and π bonds and the remaining Fe-Si bonds. Similarly, a combination of Si p_x, p_y, and p_z orbitals contribute to the Fe-Si bonds. The LDOS for both surface terminations are shown in Fig. 5. The deviations in the LDOS between the surface layers and the bulklike layer are clearly visible and are discussed in the next two subsections.

D. Relaxation of the Si-terminated surface

In Table II our results for the interlayer spacing at the Si-terminated surface are listed together with the recent results by Junquera *et al.*[10] The authors performed DFT slab calculations based on the LDA and a basis set of atomic orbitals for silicon and iron including *s*-, *p*-, and *d*-orbitals. The relaxation shows an alternating $(+-+-)$ sequence with an expansion of the spacing between the first two layers in agreement with the LEED results. The relaxation of the second- and third-layer spacings resulting from the calcula-

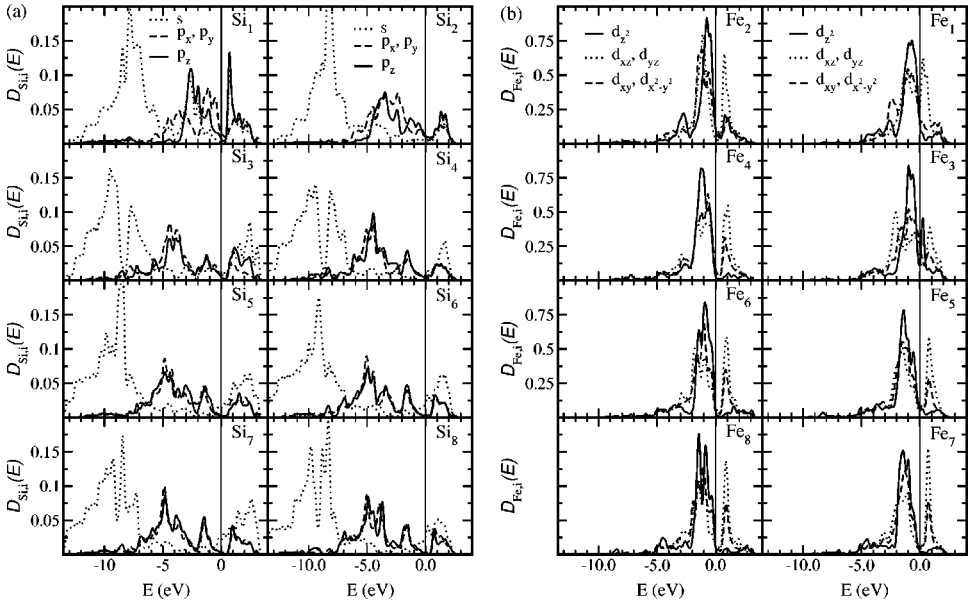

FIG. 5. Local density of states of the relaxed Si- and Fe-terminated surfaces. (a) Si LDOS: Si termination (left) and Fe termination (right). (b) Fe LDOS: Si termination (left) and Fe termination (right). The index at the element refers to the layer; i.e., Si_1 refers to the silicon surface layer of the Si-terminated surface.

tions within the GGA is larger than that obtained from the LEED analysis and the recent calculation within the LDA. The latter calculation overestimates the first-layer spacing and underestimates the relaxation below the third layer. These quantitative deviations presumably result from the different description of the Fe-Fe interaction within the LDA and GGA. However, because of the small layer spacing of the (111) surface, the absolute deviations are rather small.

A first insight into the unusual $(+-+-)$ sequence is obtained by inspecting the distances of neighboring Fe-Si and Fe-Fe pairs as given in Table III. In the following, we refer to silicon and iron layers by Si_i or Fe_i where the index counts the layers beginning with $i=1$ at the surface. The Fe-Fe distances (layer Fe_2 and Fe_4) contract by less than 1% with respect to the bulk value (2.80 Å). Also the Fe-Si distances of the surface silicon atom only slightly deviate from the corresponding bulk value (2.42 Å). They are expanded by 0.8% with respect to the adjacent iron layer (Fe_2) and by 0.4% with respect to the fourth layer (Fe_4) as indicated by dashed lines in Fig. 4(d). Basically, the alternating layer relaxation is imposed by the contraction of the Fe-Si bonds of the subsurface iron (layer Fe_2) with its four subsurface silicon neighbors (thick bond lines): the Fe-Si bonds between the Fe atom and its three Si neighbors in the third layer (Si_3) and the bond with the neighbor in the fifth layer (Si_5) are contracted by 2.5% and 3.3%. Correspondingly, the other Fe-Si bonds of these two silicon layers are elongated.

TABLE III. Theoretical results for the nearest-neighbor (Fe-Si) and second-nearest-neighbor (Fe-Fe) distances. The Fe-Si and Fe-Fe bulk distances amount to 2.42 Å and 2.80 Å. The relative deviation from the bulk values is also given. The index at the element refers to the layer in which the corresponding atom is located (for the surface layer $i=1$).

Si termination			Fe termination		
	l (Å)	$\Delta l/l_0$ (%)		l (Å)	$\Delta l/l_0$ (%)
Si_1-Fe_2	2.44	+0.8	Fe_1-Si_2	2.33	−3.7
Si_1-Fe_4	2.43	+0.4	Fe_1-Si_4	2.26	−6.6
Fe_2-Si_3	2.36	−2.5	Si_2-Fe_3	2.46	+1.7
Fe_2-Si_5	2.34	−3.3	Si_2-Fe_5	2.57	+6.2
Si_3-Fe_4	2.50	+3.3	Fe_3-Si_4	2.45	+1.2
Si_3-Fe_6	2.60	+7.2	Fe_3-Si_6	2.41	−0.7
Fe_4-Si_5	2.43	+0.4	Si_4-Fe_5	2.41	−0.4
Fe_2-Fe_4	2.78	−0.7	Fe_1-Fe_3	2.67	−4.6
Fe_4-Fe_6	2.79	−0.4	Fe_3-Fe_5	2.82	+0.7

The enhanced Fe-Si bonding that goes alongside with the relaxation is visible in the local density of states [Figs. 5(a) and 5(b)]. The largest rebonding occurs at the topmost Si layer (Si_1). From the inspection of the LDOS only, an enhancement of the Si-Fe backbonds is expected. The p_z peak at -5 eV of the LDOS of the bulklike layer (Si_7) is shifted to the region between -2.7 and -1 eV. In this region a similar feature develops in the s LDOS. This indicates towards an s-p_z hybridization that reduces the electron density above the surface and enhances the Fe-Si bond with the subsurface iron neighbor (Fe_4) underneath. A detailed analysis of the LDOS shows that there is a corresponding enhancement also in the fourth layer. At the surface, a shift of the in-plane p orbitals towards higher energies is observed additionally. A peak appears above -2 eV in the region where the LDOS of the d_{xz} and d_{yz} orbitals of the subsurface layer (Fe_2) is enhanced. This enhancement of the backbond is, however, counteracted by a reduced occupation of the p_z orbitals and the corresponding d_{z^2} orbital in layer Fe_4 by 21% and 11% as compared to the bulk. Nonetheless, the latter weakening of the backbond is not fully compensated by the increased s occupation of 11% and the s-p_z hybridization. As a result, the expansion of the Fe-Si separations of Si_1 and Si_3 with Fe_4 is rather small [dashed single bond in Fig. 4(d)]. On the other hand, the occupation of the p_x and p_y orbitals (Si_1) is reduced by 8%, while the occupation of the subsurface iron d_{xz}, d_{yz} and d_{xy}, $d_{x^2-y^2}$ orbitals increases

by only 3% and 6%, respectively. Overall, the Fe-Si bond to the subsurface layer (Fe_2) is also weakened (dashed double bond), which leads to the slightly increased layer distance.

The stronger Fe-Si bonding between the first iron subsurface layer (Fe_2) and next silicon layer (Si_3) can be explained in similar terms. There is a larger occupation of the silicon p_x and p_y orbitals (+5%) and an enhanced LDOS at energies between -5 to -4 eV and above -1 eV together with a reduced occupation of the p_z orbital (-13%). So the layer relaxation is a consequence of the stronger Fe-Si coupling (thick bond lines) between the subsurface layers Fe_2 and Si_3 and a weaker coupling (dotted bond lines) of the silicon to the iron layer Fe_6 underneath (-2% d_{z^2} occupation). The contraction of the following layer distance arises from the larger overlap in the d_{xz} and d_{yz} LDOS of layer Fe_4 with the silicon p_x and p_y orbitals of layer Si_5 as compared to the next iron layer (Fe_6).

E. Relaxation of the Fe-terminated surface

The Fe-terminated surface shows a contraction of the first-layer spacing and a $(-++-)$ relaxation sequence (cf. Table II). The considerable inward relaxation of the surface layer reduces the distance d_{12} between the surface layer and the next silicon layer to only 0.47 Å, corresponding to a relaxation of 42% in terms of the bulk distance. This relaxation is not compensated by the expansion of the distances d_{23} and d_{34} between the next three layers. Hence the Fe-Si and Fe-Fe bond lengths at the surface shrink. As stated in Table III the Fe-Si bond lengths between the surface layer and its silicon neighbors in the second and fourth layers (Si_2 and Si_4) change by -3.7% and -6.6%. Also the Fe-Fe bond lengths between the surface layer and the third layer (Fe_3) are reduced by 4.6%. Following the $(-++-)$ sequence, elongated Fe-Si bonds are found between the third layer (Fe_3) and its silicon neighbors (Si_2: +1.7%; Si_4: +1.2%). The relaxation of the other bond distances, in particular for the Fe-Fe bond between the layers Fe_3 and Fe_5, is less pronounced (0.7%).

A similar but smaller relaxation for the first two layer spacings was found by Junquera *et al.* within the LDA.[10] However, they obtained a different $(-+--+)$ relaxation sequence. This is possibly related to the fact that the LDA does not consider a magnetic ordering at the surface. On the contrary, our GGA calculations clearly show a substantial magnetic moment at the Fe-terminated surface.

The occurrence of surface magnetism is the most striking property of the Fe-terminated surface. The magnetic moment is located at the surface layer (Fe_1) and to a smaller extent at the third layer (Fe_3). It amounts to $1.8\mu_B$ per surface unit cell. The largest contribution (68%) stems from the d_{xz}/d_{yz} orbitals at the surface layer. The remaining moment is distributed mainly among the surface orbitals $d_{x^2-y^2}$, d_{xy}, and the third-layer d_{z^2} orbital ($\approx 8\%$ each).

An exchange splitting of the LDOS occurs at the d_{xz}/d_{yz} peak in the surface layer and at the d_{z^2} peak at the Fe_3 layer. The peak associated with the minority-spin states appears above the Fermi level, whereas the peak of the majority-spin states is located below. A pseudogap at the Fermi level is clearly visible in Fig. 5(b). The opening of the pseudogap can be qualitatively understood as follows. Due to the interaction with the potential energy barrier at the surface, the bulk LDOS peaks at about -1.5 eV are shifted towards the Fermi level. On the other hand, due to the missing neighbors, the antibonding d_{xz}/d_{yz} peak lowers its energy such that the Fermi level falls into the region of a high LDOS. This corresponds to a cancellation of the crystal-field splitting at the surface. A ferromagnetic ordering then splits the LDOS at the Fermi level. The exchange splitting is lower for the other orbitals at the surface, but it is clearly visible in the spin-resolved LDOS. As a result of the splitting, a depopulation of the d orbitals occurs. The d_{z^2} occupation at the Fe_3 layer is reduced by 13% as compared to the bulk. Despite the strong interaction with the surface barrier, the occupation at the surface layer changes only by -4% (d_{xz},d_{yz}), -3% (d_{z^2}), and -2% (d_{xy},$d_{x^2-y^2}$). Basically, the relaxation is driven by an enhancement of the Fe-Si and Fe-Fe backbonds of the iron surface layer (Fe_1). At the surface layer and the third layer (Fe_3) a peak appears between -3 and -2 eV below the main peak (Fe_1: $d_{xy}/d_{x^2-y^2}$ and d_{z^2}; Fe_3: d_{xz}/d_{yz}). In this region similar features develop in the p LDOS of the adjacent Si layers. The overlap of these features with the LDOS of the surface layer is more pronounced than with the third layer. Thus, covalent aspects dominate in the relaxation of the Fe-terminated surface similar to our findings for the Si termination described in the previous section.

IV. DISCUSSION

The quantitative LEED analysis presented in this paper for c-FeSi-films on Si(111) clearly indicates a Si termination of the surface and reveals a structural relaxation that is in quantitative agreement with the theoretical results. On the basis of the evaluation of the surface tensions our calculations predict that the Si termination is the preferred surface termination in equilibrium between the surface and the substrate. In the experiment equilibrium is reached by a prolonged annealing at a temperature of 300 °C. This situation can be regarded as a diffusive balance between the film and substrate, which serves as an infinite, yet kinetically limited Si reservoir. Thermodynamically, this corresponds to the saturation value for the chemical potential μ_{Si}, i.e., $\Delta\mu_{Si} \approx 0$.

Recently, an alternative preparation, the deposition of a Fe film on the Si substrate and a subsequent solid-state reaction, has been demonstrated to lead also to high-quality c-FeSi-films.[11] Similar structural results as in the present study were found for this film, in particular an unambiguous Si termination. This corroborates the theoretical prediction that for slight deviations from the equilibrium with the substrate, a Fe-terminated surface should still not develop. Only if kinetic aspects suppress the equilibrium with the substrate (which is not expected in the analyzed films) may the Fe-terminated surface be realized. Nevertheless, it is feasible that under preparation conditions far off the equilibrium, it may be possible to generate a situation that is better represented by a higher μ_{Fe}.

Yet, as mentioned in Sec. III, such Fe-rich conditions

could also lead to other Fe-rich silicide phases such as the well-known Fe_3Si. Indeed, it should be noted that for bulk Fe_3Si crystals a temperature-dependent reversible phase transformation between the $D0_3$ bulk structure and the present *c*-FeSi phase was recently discovered at low-index surfaces.[41] Higher temperatures, at which Si is known to segregate to the surface, lead to the *c*-FeSi phase in agreement with the findings of the present paper. Concerning the case of FeSi films on Si(111), definitely the equilibrium Si termination will be established if a well-ordered (1×1) LEED pattern develops upon annealing according to the recipes used in the present experiments. So the reason for our result being at variance with the iron termination obtained by ion scattering and electronic structure measurements[6] is not clear. Interestingly, a recent reexamination of the same electronic structure data[10] has been found to favor silicon instead of iron termination. So possibly the ion scattering data were misinterpreted which can easily happen as for quantitative data evaluation atomic cross sections and the surface geometry must be known with sufficient accuracy. On the other hand, it might also be that the film investigated had not yet reached equilibrium with the substrate and some disordered Fe exists at the surface.

The surface relaxation of the Si-terminated surface is characterized by an alternating layer relaxation in a $(+-+-)$ sequence. The detailed bond analysis shows that covalent atomic bonds dominate and guide the layer arrangement. With the covalent bonding we also explain the inward relaxation of the Fe-terminated surface. The relaxation pattern and the driving mechanism are unusual for typical (111) metal surfaces. There, the compression of the outermost layer distances originates[42] from the Smoluchowski smoothening[43] of the delocalized electron density at the surface. The dominance of either mechanism is not readily apparent as illustrated, for example, by the aluminum surfaces. On Al(111) and Al(100) a small outward relaxation is found.[44] This relaxation has been also verified by DFT-LDA calculations.[45,46] It recently was explained theoretically[47] by an increased *p*-orbital-like character of the surface density of states at the Fermi level. For the (111) and (100) surface orientations the larger energetic splitting of the in-plane *p* orbitals from the *p* orbital perpendicular to the surface and the reduced occupation of the latter was shown to lead to the observed effects.

Finally, for the Fe terminated surface a magnetic moment in the topmost two layers was found theoretically. Experimentally, an Fe-termination may be achieved by a kinetically controlled preparation procedure such as limited annealing times or supplying a Fe background evaporation during the annealing process. Magnetic measurements have indeed been carried out for thicker epitaxial $Fe_{1+x}Si_{1-x}$ films,[48] leading to the result that if the CsCl structure is not reached in ideal stoichiometry, i.e., in Fe-rich CsCl films, a magnetic moment persists. In this case the ferromagnetism can certainly be viewed as bulk effect, yet based on an Fe-enriched structural situation. However, even for ultrathin films ferromagnetic behavior could be found in a recent x-ray absorption experiment provided that the films were not annealed until a well-ordered (1×1) pattern was observed in LEED.[49] This latter experiment seems to represent the nonequilibrium situation of kinetically hindered Si diffusion, i.e., a more iron-rich situation in analogy to the increased chemical potential μ_{Fe} as discussed in Sec. III E.

V. CONCLUSION

Using experimental and theoretical methods, namely, quantitative LEED and *ab initio* DFT-GGA calculations, the equilibrium surface termination of *c*-FeSi thin films on Si(111) is unambiguously determined to be a Si layer of the CsCl-type film structure. Quantitative agreement between experiment and theory is achieved for the layer distances in the surface slab. Down to the fourth-layer spacing we find an alternating relaxation starting with an expansion at the surface. The driving force behind this unusual relaxation stems from the enhanced covalent bonding between the subsurface iron and silicon layers. From energetic arguments we conclude that an Fe termination should not be realized when quasiequilibrium between the substrate and the film surfaces is achieved.

ACKNOWLEDGMENT

Support by the Deutsche Forschungsgemeinschaft through Grant Nos. SFB292 and He1502/8-1 is gratefully acknowledged.

[1] S. P. Murarka, *Silicides for VLSI Applications* (Academic, Orlando, FL, 1983).
[2] O. Kubaschewski, *Iron Binary Phase Diagrams* (Springer, Berlin, 1982).
[3] E. G. Moroni, R. Podloucky, and J. Hafner, Phys. Rev. Lett. **81**, 1969 (1998).
[4] H. von Känel, K. A. Mäder, E. Müller, N. Onda, and H. Sirringhaus, Phys. Rev. B **45**, 13 807 (1992).
[5] U. Kafader, M. H. Tuilier, C. Pirri, P. Wetzel, D. Gewinner, D. Bolmont, O. Heckmann, C. Chandesris, and H. Magnan, Europhys. Lett. **22**, 529 (1993).
[6] J. J. Hinarejos, G. R. Castro, P. Segovia, J. Alvarez, E. G. Michel, R. Miranda, A. Rodríguez-Marco, D. Sánchez-Portal, E. Artacho, F. Ynduráin, S. H. Yang, P. Ordejón, and J. B. Adams, Phys. Rev. B **55**, 16 065 (1997).
[7] E. G. Moroni, W. Wolf, J. Hafner, and R. Podloucky, Phys. Rev. B **59**, 12 860 (1999).
[8] S. Walter, M. Krause, F. Blobner, S. Müller, U. Starke, and K. Heinz (unpublished).
[9] M. Fanciulli, G. Weyer, A. Svane, N. E. Christensen, H. von Känel, E. Müller, N. Onda, L. Miglio, F. Tavazza, and M. Celino, Phys. Rev. B **59**, 3675 (1999).
[10] J. Junquera, R. Weht, and P. Ordejón, Surf. Sci. **482**, 625 (2001).
[11] U. Starke, W. Weiss, M. Kutschera, R. Bandorf, and K. Heinz, J. Appl. Phys. **91**, 6154 (2002).
[12] K. Heinz, Rep. Prog. Phys. **58**, 637 (1995).

[13] V. Blum and K. Heinz, Comput. Phys. Commun. **134**, 392 (2001).
[14] P. J. Rous, J. B. Pendry, D. K. Saldin, K. Heinz, K. Müller, and N. Bickel, Phys. Rev. Lett. **57**, 2951 (1986).
[15] P. J. Rous and J. B. Pendry, Surf. Sci. **219**, 355 (1989); **219**, 373 (1989).
[16] P. J. Rous, Prog. Surf. Sci. **39**, 3 (1992).
[17] M. Kottcke and K. Heinz, Surf. Sci. **376**, 352 (1996).
[18] J. Pendry, J. Phys. C **13**, 937 (1980).
[19] S. Walter, V. Blum, L. Hammer, S. Müller, K. Heinz, and M. Giesen, Surf. Sci. **458**, 155 (2000).
[20] J. Rundgren, Phys. Rev. B **59**, 5106 (1999).
[21] J. Rundgren (private communication).
[22] D. W. Jepsen, Surf. Rev. Lett. **6**, 627 (1999).
[23] N. Onda, H. Sirringhaus, S. Goncalves-Conto, C. Schwarz, S. Zehnder, and H. von Känel, Appl. Surf. Sci. **73**, 124 (1993).
[24] F. Jona and P. M. Marcus, in *The Structure of Surfaces II*, Springer Series in Surface Science, Vol. 11, edited by J. F. van der Veen and M. A. Van Hove (Springer, Berlin 1988), p. 90.
[25] J. Sokolov, F. Jona, and P. M. Marcus, Phys. Rev. B **33**, 1397 (1986).
[26] M. Arnold, A. Fahmi, W. Frie, L. Hammer, and K. Heinz, J. Phys.: Condens. Matter **11**, 1673 (1999).
[27] L. Hammer, M. Kottcke, M. Taubmann, S. Meyer, C. Rath, and K. Heinz, Surf. Sci. **431**, 220 (1999).
[28] M. Bockstedte, A. Kley, J. Neugebauer, and M. Scheffler, Comput. Phys. Commun. **107**, 187 (1997).
[29] J. P. Perdew, J. A. Chevary, S. H. Vosko, K. A. Jackson, M. R. Pederson, D. J. Singh, and C. Fiolhais, Phys. Rev. B **46**, 6671 (1992) and references therein.
[30] M. Fuchs and M. Scheffler, Comput. Phys. Commun. **119**, 67 (1999).
[31] M. Fuchs, M. Bockstedte, E. Pehlke, and M. Scheffler, Phys. Rev. B **57**, 2134 (1998).
[32] J.-H. Cho and M. Scheffler, Phys. Rev. B **53**, 10 685 (1996).
[33] Cutoff radii for the silicon pseudopotential: $r_s = 1.7$ a.u., $r_p = 1.7$ a.u., and $r_d = 2.0$ a.u.
[34] M. Fuchs (unpublished).
[35] Cutoff radii for the soft iron pseudopotential ps1: $r_s = 2.2$ a.u., $r_p = 2.4$ a.u., and $r_d = 2.5$ a.u.
[36] Cutoff radii for the harder iron pseudopotential ps2: $r_s = 1.8$ a.u., $r_p = 2.4$ a.u., and $r_d = 1.8$ a.u.
[37] F. R. de Boer *et al.*, in *Cohesion in Metals*, edited by F. R. de Boer and D. G. Pettifor (North-Holland, Amsterdam, 1988), Vol. 1.
[38] H. J. Monkhorst and J. D. Pack, Phys. Rev. B **13**, 5188 (1976).
[39] K. A. Mäder, H. von Känel, and A. Baldereschi, Phys. Rev. B **48**, 4364 (1993).
[40] The radial atomic pseudowave function is cut off by a steplike function at 1.5 a.u. for Si and 1.8 a.u. for Fe. The LDOS is consistently calculated using the atomic pseudowave functions of the slab calculation.
[41] U. Starke, J. Schardt, W. Weiss, W. Meier, C. Polop, P. L. de Andres, and K. Heinz, Europhys. Lett. **56**, 822 (2001).
[42] M. W. Finnis and V. Heine, J. Phys. F: Met. Phys. **4**, L37 (1974).
[43] R. Smoluchowski, Phys. Rev. **60**, 661 (1941).
[44] J. R. Noonan and H. L. Davis, J. Vac. Sci. Technol. A **8**, 2671 (1990).
[45] K. P. Bohnen, J. Schöchlin, and K. M. Ho, Surf. Sci. **324**, 113 (1995).
[46] R. Stumpf and M. Scheffler, Phys. Rev. B **53**, 4958 (1996).
[47] C. J. Fall, N. Binggeli, and A. Baldereschi, Phys. Rev. B **58**, 7544 (1998).
[48] D. Berling, G. Gewinner, M. C. Hanf, K. Hricovini, S. Hong, B. Loegel, A. Mehdaoui, C. Pirri, M. H. Tuilier, and P. Wetzel, J. Magn. Magn. Mater. **191**, 331 (1999).
[49] U. Starke, A. Kumar, M. Tallarida, and K. Horn (unpublished).